repeats were obtained by repetitive subcloning of the *Hin*dIII/*Bam*HI fragment with molecular weight higher than that of the major band visualized in the gel. The resulting colonies were screened by PCR with primers as previously described (Mangiarini *et al.* 1996). The CAG repeat number was verified by sequencing (BigDye Terminator Cycle Sequencing kit; Applied Biosystems, Foster City, CA, USA) and by microsatellite analysis on ABI 3700 using GeneScan 3.7.1 software (Applied Biosystems). Clones containing expanded CAG repeats were selected for further use. A *Hin*dIII/*Not*I fragment from this plasmid (containing exon 1 and EGFP) was introduced into pBluescript-KS vector. The huntingtin promoter was ligated to the *Pst*I and *Stu*I/*Sma*I ends. SV40 polyadenylation signal was added to the *Sac*II site. The final construct was microinjected into (C57BL/6:DBA2) fertilized eggs.

Mouse genotyping and copy number of transgene

Genomic DNA was extracted from mouse tail biopsies by the phenol/chloroform method using the NA-1000 automatic isolation system (Kurabo, Osaka, Japan) and genotyping by PCR was performed as described earlier (Mangiarini *et al.* 1996). From mice carrying the transgene, two founder lines of transgenic mice were selected and backcrossed to C57BL/6J. All mice used in these experiments were heterozygous for transgene and male.

To assess the copy number of the transgene in the transgenic mice, TaqMan quantitative RT-PCR was performed using the probe-primer set specific for *EGFP* and TaqMan Rodent glyceraldehyde-3-phosphate dehydrogenase (GAPDH) Control Reagents (Applied Biosystems) for the internal control, on an ABI7700 thermal cycler (Applied Biosystems) as described previously (Tateno *et al.* 2004). The *EGFP* copy numbers in HD190QG ($n = 3$) and HD150QG ($n = 3$) were thus calculated as 2.46 ± 0.55 and 10.37 ± 0.38 copies (mean ± SD), respectively.

Immunohistochemistry

Frozen brains mounted in Tissue-Tek were sectioned using a freezing microtome (20 μm thickness). Sections were fixed with 4% paraformaldehyde in phosphate-buffered saline for 20 min, washed several times, blocked with 5% non-fat dried milk for 1 h and then incubated overnight with primary antibody. In some cases, after fixation, the sections were washed with phosphate-buffered saline, stained with propidium iodide, mounted in 50% glycerol and observed under a confocal microscope (TCS SP2; Leica Microsystems, Wetzlar, Germany). Staining was also carried out using an ABC Elite kit (Vector Laboratories, Burlingame, CA, USA) for light microscopic observation. For confocal microscopic observation, staining was performed using the appropriate CY3-labeled secondary antibody and then mounted with antifade solution (Vectashield Mounting Media; Vector Laboratories). We used primary antibodies against the N-terminal part of huntingtin (goat polyclonal; Santa Cruz Biotechnology, Santa Cruz, CA, USA), ubiquitin (Dako Japan Co., Kyoto, Japan), GFP (rabbit polyclonal; Molecular Probes, Eugene, OR, USA), neuron-specific nuclear protein (NeuN) (Chemicon International, Temecula, CA, USA) and secondary antibodies conjugated with CY3 (Molecular Probes) at a 1 : 500 dilution.

Electron microscopy

Mice were anesthetized with diethyl ether and then perfused intracardically with 0.1 M cacodylate buffer containg 2.5% glutaraldehyde and 1% paraformaldehyde, pH 7.4. Brains were removed and immersed in the same mixture for 10 days. The tissue blocks of the coronally sliced dorsal neocortex and dentate gyrus and of the mid-sagittally sliced cerebellar vermis were post-fixed in 1% osmium tetroxide, dehydrated through a graded ethanol series and then embedded in Epon 812. Toluidine blue-stained 1-μm-thick sections were examined with a light microscope. Ultrathin sections of the dorsal neocortex, dentate gyrus and vermis were stained with lead citrate and uranyl acetate and then examined under an electron microscope at 100 kV (H-9000; Hitachi, Tokyo, Japan).

Subcellular fractionation

Mouse brains were homogenized in nine volumes (w/v) of 0.25 M sucrose/buffer A (50 mM Tris-HCl, pH 7.4, 5 mM $MgCl_2$, 2 mM dithiothreitol and 1 mM phenylmethylsulfonyl) supplemented with Complete EDTA-free protease inhibitor cocktail tablets (Roche Diagnostics, Mannheim, Germany) in a digital homogenizer (As One, Osaka, Japan) using eight strokes at 1000 r.p.m. A portion of the homogenate was briefly sonicated and used as the total lysate and the rest of the homogenate was centrifuged at 600 *g* for 10 min at 4°C. The pellets were resuspended and homogenized in 5 mL of 2.1 M sucrose/buffer A by five strokes at 1000 r.p.m. with the digital homogenizer. Nuclei were sedimented by centrifugation at 8000 *g* for 80 min at 4°C. The pellet containing the nuclei was resuspended in 0.2 mL of 10 mM Tris-HCl (pH 7.4) and 2 mM $MgCl_2$ with the protease inhibitors.

Immunoblotting

Proteins were separated by sodium dodecyl sulfate–polyacrylamide gel electrophoresis and transferred onto polyvinylidene fluoride membranes (Immobilon-P; Millipore, Bedford, MA, USA). The membranes were incubated in blocking buffer [5% skim milk in TBST (50 mM Tris-HCl, pH 7.5, 0.15 M NaCl, 0.05% Tween20)] with primary antibody in TBST and then with horseradish peroxidase-conjugated secondary antibody (Amersham Biosciences, Piscataway, NJ, USA) in TBST. Detection was carried out with enhanced chemiluminescence reagent (Amersham Biosciences). The primary antibodies used in the immunoblotting experiments were obtained from the following sources: mouse monoclonal antibody 1C2 and GAPDH from Chemicon International and goat polyclonal lamin B from Santa Cruz Biotechnology. All primary antibodies were used at a 1 : 1000 dilution for immunoblotting.

Direct observation of expanded polyglutamine-EGFP in transgenic mouse brains by a fluorescent imager

Frozen brains mounted in Tissue-Tek were sectioned using a freezing microtome (10 μm thickness). Sections were directly observed with a laser-scanning imaging system (Molecular Imager FX; Bio-Rad Laboratories, Hercules, CA, USA) with a 488-nm external Ar ion laser (Gingrich *et al.* 2000). Sections were imaged using the 488-nm laser with the standard 530 ± 30 nm bandpass emission filter (530DF30; Omega Optical, Brattleboro, VT, USA).

RNA extraction, preparation of labeled cRNA and array hybridization

RNA was extracted from the cerebrum of transgenic mice using TRIzol reagent (Invitrogen, Carlsbad, CA, USA) according to the manufacturer's protocol. Poly $(A)^+$ RNA was isolated from the

samples using μMACS mRNA Isolation kit (Miltenyi Biotech, Auburn, CA, USA). Biotinylated cRNAs were prepared according to the Affymetrix (Santa Clara, CA, USA) protocol. Mu11K and U-74 oligonucleotide arrays (Affymetrix) were pre-hybridized, hybridized, washed and stained as recommended by the manufacturer using a GeneChip Fluidics Station 400 (Affymetrix).

Microarray gene expression analysis

Four independent pair-wise comparisons were performed using MAS 5.0 software (Affymetrix) to evaluate gene expression changes in HD190QG and R6/2 when compared with their littermate controls. Difference calls were scored and only mRNAs that received difference calls in the same direction (increased or decreased) in at least three of the four pair-wise comparisons were included for presentation in the present study.

Verification of differential expression by real time TaqMan RT-PCR

We synthesized the TaqMan primer and probe sets with the Primer Express Software (Applied Biosystems). The nucleotide sequence of the primers is shown in supplementary Table S1. Total RNA was extracted from mice brains using TRIzol reagent. Contaminating genomic DNA was removed with RNase-free DNase I (Takara Bio, Shiga, Japan). Complementary DNAs were synthesized using TaqMan Reverse Transcription Reagents (Applied Biosystems). We used 1 μg of total RNA for the 100-μL reaction. The TaqMan PCR reaction was performed as follows. We used 15 μL of TaqMan Universal PCR Master Mix (Applied Biosystems) for the 30-μL reaction. Primers and probes were added in optimal concentrations. We used 1 μL of RT mix for each PCR. PCR conditions were standard for the 7700 Sequence Detector System (Applied Biosystems): 2 min at 50°C, 10 min at 95°C followed by 40 cycles of 95°C for 15 s and 60°C for 1 min. The mRNA quantity for the gene of interest was normalized by the quantity of 18S rRNA in each sample. Statistical comparisons of TaqMan RT-PCR were carried out by Student's *t*-test.

In situ hybridization

We used IMAGE 2938032 (DARRP-32), IMAGE 640127 (oxytocin), IMAGE 16180045 (vasopressin) and IMAGE 466874 (CART) clones (Invitrogen) to synthesize probes. EGFP cDNA was amplified by PCR from pEGFP-N1 (BD Biosciences) vector using oligonucleotide primers of 5′-ATGGTGAGCAAGGGCGAGGA GCTG-3′ and 5′-TTACTTGTACAGCTCGTCCATGCC-3′. The fragments were subcloned into pGEM-T Easy™ vector (Promega, Madison, WI, USA). The IMAGE clones and the plasmid with EGFP cDNA were used as templates for *in vitro* transcription of digoxigenin-labeled riboprobes (Roche Molecular Biochemicals, Indianapolis, IN, USA) using T3, T7 and SP6 RNA polymerases (Invitrogen). Sections were hybridized *in situ* using non-radioactive digoxigenin-labeled cRNA probes essentially as described previously (Nagai *et al.* 1997).

Counting of oxytocin-expressing neurons and neuronal nuclei in the hypothalamus

Serial-cut frozen sections (20 μm) were used for *in situ* hybridization of oxytocin mRNA and immunohistochemistry with an antibody to NeuN (Chemicon International). We adjusted the contrast and brightness of the digital images so that the oxytocin-expressing neurons and the anti-NeuN antibody stained only neuronal nuclei and counted the number of neurons with a MacSCOPE program (Mitani, Tokyo, Japan).

Results

Expanded polyglutamine-EGFP transgenic mice exhibit progressive behavioral and motor abnormalities and shorter life spans

We generated two lines of transgenic mice that expressed expanded polyQ-EGFP fusion protein under the control of the human huntingtin promoter. The transgene construction is shown in Fig. 1(a). One line contains a construct including two main fragments, one having 190 CAG repeats and the other 155, whereas the other line contains a construct including three polymorphic fragments with a CAG repeat number around 150, 120 and 33, respectively (Fig. 1b). The genotyping results of R6/2 and R6/1 lines, containing 145 and 130 CAG repeats, respectively, were included side by side in the same PCR amplification for comparison. We named these new HD transgenic lines based on the highest number of CAG repeats and the presence of EGFP and they were therefore designated HD190QG and HD150QG (Q-glutamine; G-EGFP), respectively.

Although both lines of transgenic mice showed progressive motor and behavioral deficits with a shorter life span compared with their littermate controls, they differed in the time of disease onset, severity and survival rate. Median survival values for HD190QG and HD150QG were 21 and 32 weeks, respectively (Fig. 1c). The motor and behavioral symptoms included fine tremor, chorea-like movements, ataxic gait and clasping of the limbs when held by the tail. These symptoms were similar to those of R6/2 mice (Mangiarini *et al.* 1996). The onset of motor symptoms such as fine tremor and ataxic gait was around 5–6 weeks for HD190QG and 9–11 weeks for HD150QG mice. At around 8 weeks (HD190QG) and 16 weeks (HD150QG), the mice started to show irregular, jerky involuntary head movements which were similar to chorea. These symptoms progressively worsened. At around 16 weeks (HD190QG) and 30 weeks (HD150QG), the mice had difficulty in walking because of severe ataxia and some of the HD190QG and HD150QG mice showed clasping of limbs but the clasping phenomenon was rarely observed compared with R6/2 mice. All 20 HD190QG and 79 HD150QG mice were dead by 25 and 58 weeks, respectively, whereas all 36 mice in the control groups for HD190QG and HD150QG were alive and healthy.

Expression of the transgene was monitored using 1C2 antibody, which selectively recognizes expanded polyQ tracts (Trottier *et al.* 1995). As shown in Figs 1(d and e), the 1C2 antibody detected two bands in brain samples from both the HD190QG and HD150QG transgenic mice and also

in various tissues that have the corresponding genotype. The band corresponding to the 33 CAG repeats in HD150QG was missing because 1C2 only recognizes expanded polyQ. We also confirmed transgene expression using an antibody against either EGFP or N-terminal huntingtin (data not shown).

Visualization of expanded polyglutamine protein aggregation

The mice of both lines displayed progressive neurological phenotypes. As HD150QG mice showed a gradual progression of neuropathology when compared with HD190QG mice, we checked expression of the transgene in different parts of the brain of HD150QG by examining EGFP fluorescence using confocal microscopy. Sections collected from 35-week-old HD150QG mice were fixed with paraformaldehyde and stained with propidium iodide, as described in Materials and methods, and were observed under a confocal microscope. The majority of dense EGFP-positive aggregates were detected in the striatum, cortex and hippocampus of the transgenic mouse brain and most of the green fluorescence was localized in the cytoplasm while only a few aggregates were detected in the nucleus (Fig. 2a, i–iii). The progressive hippocampal pathology in the R6/2 mouse has been well described (Morton *et al.* 2000; Meade *et al.* 2002). The section at low magnification shows the distribution of EGFP in the whole hippocampus (Fig. 2a, iv). Almost all the EGFP-positive aggregates were in the cytoplasm in the older mice.

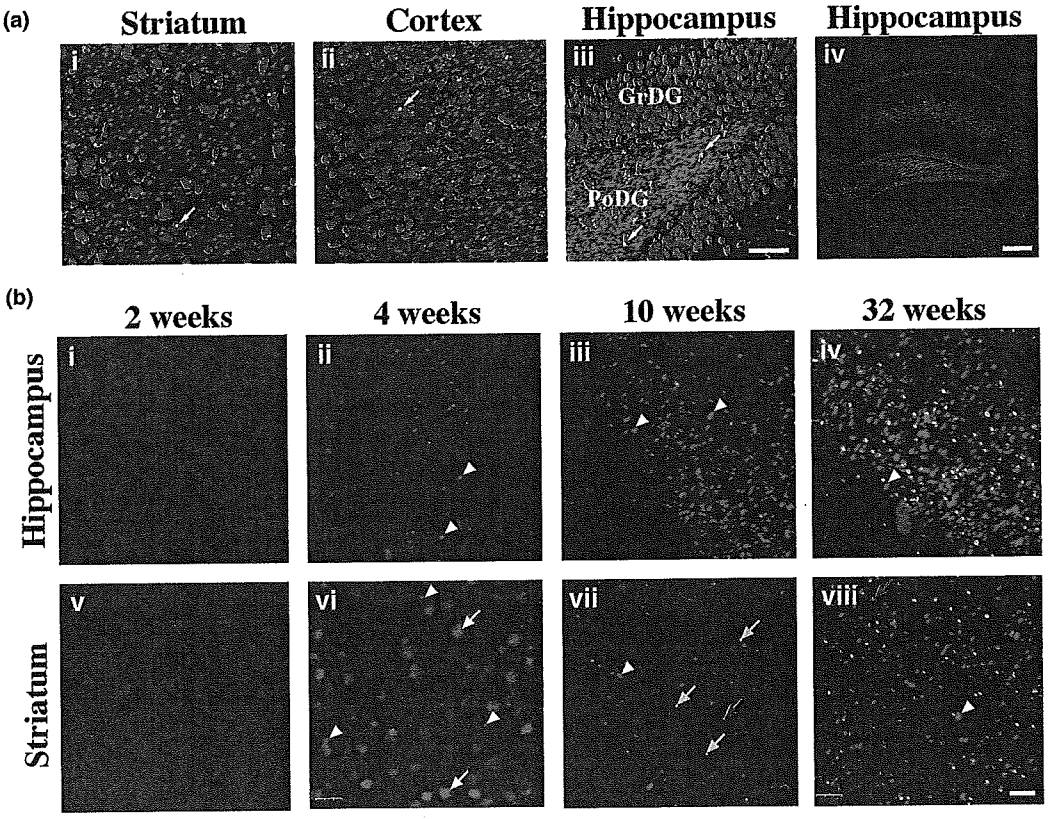

Fig. 2 Direct visualization and age-dependent changes in the formation of cytoplasmic and nuclear aggregates of human expanded polyglutamine (polyQ)-EGFP fusion proteins in HD150QG mice. Frozen brain sections from 35-week-old HD150QG mice were observed under a confocal microscope. (a) The green fluorescent dots represent the aggregates of the transgene product (expanded polyQ-EGFP) and localize mostly in the cytoplasm. The yellow arrow indicates a green fluorescent aggregate that appears in the nucleus stained with propidium iodide (red). The striatum, cerebral cortex and hippocampus are shown in (i–iii), respectively. GrDG, granular layer, dentate gyrus; PoDG, polymorph layer, dentate gyrus. Scale bar, 20 μm. Low magnification view of section from hippocampus is shown in (iv). Scale bar, 200 μm. (b) Frozen sections from HD150QG mice at different ages were subjected to immunofluorescence staining of ubiquitin. Ubiquitin was labeled with CY3-conjugated secondary antibody and the overlapping images of green (diffuse or aggregated transgene product) and red (ubiquitinated aggregates) were collected and merged. (i–iv) Hippocampus; (v–viii) striatum. (i and v) 2 weeks; (ii and vi) 4 weeks; (iii and vii) 10 weeks; (iv and viii) 32 weeks. The yellow arrow indicates the ubiquitin-positive nuclear aggregates that retained EGFP fluorescence, while the red arrow represents the ubiquitin-positive nuclear aggregates that totally lost EGFP fluorescence. White arrowheads indicate cytoplasmic aggregates and white arrows indicate nuclear-accumulated transgene product or their aggregates.

Expanded polyglutamine-EGFP cytoplasmic and nuclear aggregates appear simultaneously

Brains from HD150QG transgenic mice of different ages were stained for ubiquitin and visualized by fluorescence microscopy. Although no fluorescent aggregates were observed in 2-week-old mice (Fig. 2b, i and v), EGFP-positive cytoplasmic aggregates were observed in the hippocampal area in mice of about 4 weeks old, which is the same age that nuclear accumulation of EGFP fluorescence with few EGFP-positive aggregates was seen in the striatum (Fig. 2b, ii and vi). With increasing age, the number of cytoplasmic aggregates increased, while the nuclei gradually lost EGFP fluorescence. The ubiquitin antibody detected large nuclear aggregates in 10-week-old mice. Some of these ubiquitin-positive nuclear aggregates also exhibited EGFP fluorescence, which gradually disappeared with increasing age (Fig. 2b, iii and vii). The ubiquitin antibody also detected cytoplasmic aggregates but they were sometimes obscured by the intense EGFP fluorescence and were difficult to see. We have also noticed that the EGFP-positive cytoplasmic and nuclear aggregates appeared almost simultaneously and that they initially appeared in the striatum and hippocampus at around 4 weeks of age.

Ubiquitin-positive nuclear aggregates lose EGFP fluorescence and undergo proteolytic processing

As older transgenic mice showed cytoplasmic accumulation of EGFP aggregates, we further monitored age-dependent aggregate formation using the fluorescence of EGFP as well as antibodies against ubiquitin and N-terminal huntingtin. We performed immunofluorescence as well as immunohistochemical staining for ubiquitin in brains from 32- to 35-week-old HD150QG mice. Although EGFP fluorescence was not lost after 4% paraformaldehyde fixation, it was completely lost after immunohistochemical staining by diaminobenzidine (DAB) and subsequent mounting. The ubiquitin antibody detected large nuclear aggregates (Fig. 3a, i–vi) similar to those found in R6/2 HD transgenic mice (Davies *et al.* 1997). Some of the ubiquitin-positive nuclear aggregates also retained weak EGFP fluorescence. Electron microscopic analysis revealed the frequent presence of dark neurons (Fig. 3a, vii) in the hippocampus and further confirmed the presence of nuclear aggregates (Fig. 3a, viii). The presence of similar dark neurons has been reported in the R6/2 transgenic mouse (Turmaine *et al.* 2000).

To determine why EGFP fluorescence is lost in the nuclear aggregates, we collected brain samples from transgenic mice of different ages and isolated the nuclear fraction for the detection of the transgene product by anti-GFP and 1C2 antibodies. GFP antibody-positive sodium dodecyl sulfate-insoluble polyQ-EGFP fusion proteins were not only detected around 75 kDa but also at the top of the gel (Fig. 3b). These GFP-immunoreactive aggregates (gel-excluded materials) were concentrated in the nuclear fraction (which also included cytoplasmic aggregates) and were age-dependently increased. On the other hand, sodium dodecyl sulfate-soluble polyQ-EGFP fusion proteins detected by 1C2 antibody were age-dependently decreased (Fig. 3b).

To further confirm the nuclear accumulation of the transgene product, we examined transgenic mouse brain sections immunostained with polyclonal antibody against N-terminal huntingtin and EGFP. As shown in Fig. 3(c), the N-terminal huntingtin antibody strongly detected most of the nuclear aggregates as well as cytoplasmic aggregates. This finding was confirmed by double immunofluorescence staining using ubiquitin and N-terminal huntingtin antibody (data not shown). However, anti-GFP polyclonal antibody detected a few of the nuclear aggregates (weak staining) and most of the cytoplasmic aggregates that exhibited EGFP fluorescence (Fig. 3c). This result suggests that expanded polyQ-EGFP fusion proteins and their aggregates are undergoing proteolytic processing in the EGFP part in nuclei and losing EGFP fluorescence.

Visualization of cytoplasmic expanded polyglutamine-EGFP aggregates in transgenic mice brains using a fluorescent imager

The distribution of expanded polyQ-EGFP aggregates in the brain was analysed using a fluorescent imager. Brain sections from HD190QG mice were prepared and EGFP fluorescence was directly observed as described in Materials and methods. Macroscopic analysis indicated that EGFP fluorescence was very weak but detectable at 4 weeks in brain sections of HD190QG mice (Fig. 4a). The fluorescence was first detected in the hippocampus. EGFP fluorescence became widespread, increased with age and occurred at a much higher frequency in the striatum, hippocampus and hypothalamus in the brains of 12–24-week-old HD190QG mice (Fig. 4a).

Widespread transgene expression in HD190QG mice

The expression of expanded polyQ-EGFP mRNA was examined in whole brain sections by *in situ* hybridization using an EGFP probe (Fig. 4b). Expression of the transgene in the striatum, hippocampus, cortex and hypothalamus was intermediate. Macroscopically, the expression level correlates with neuronal cell density. In contrast, no positive signal was observed in littermate control brains, confirming the specificity of the EGFP probe for *in situ* hybridization. These results clearly indicate that there is no correlation between transgene expression and aggregate formation in the striatum, hippocampus, cortex and hypothalamus.

GeneChip profiling

Our transgenic mice exhibited progressive behavioral and motor abnormalities and formed expanded polyQ-EGFP cytoplasmic and nuclear aggregates. To examine the neural responses to expanded polyQ expression and aggregate formation *in vivo*, we carried out comprehensive analysis of the altered or compensatory gene expression using a

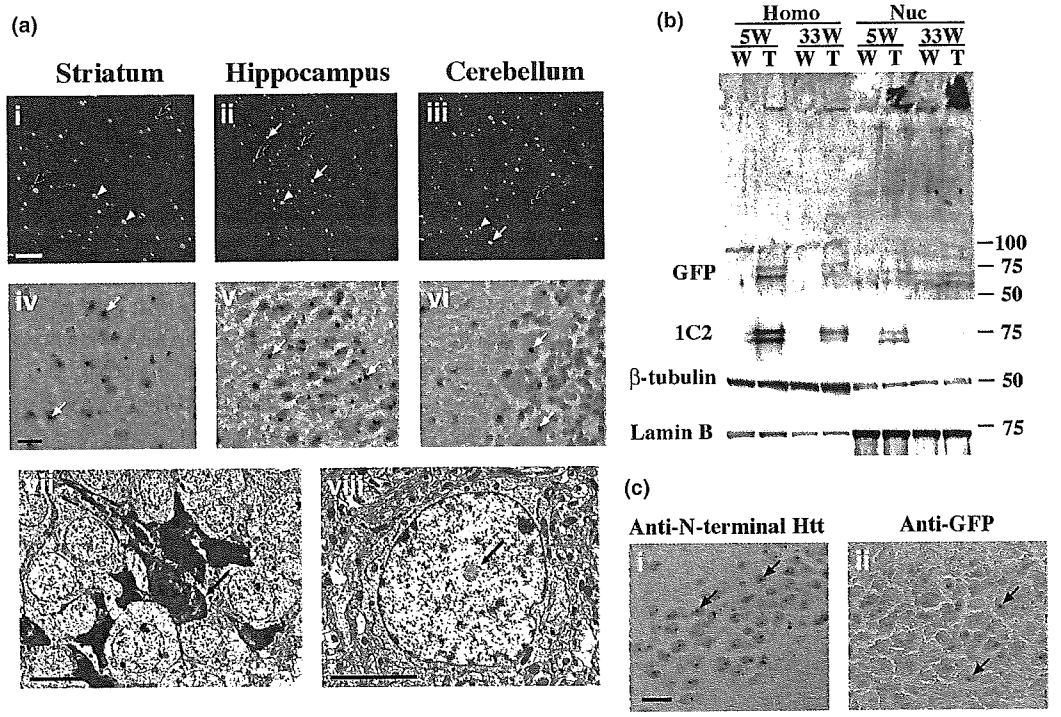

Fig. 3 Analysis of cytoplasmic and nuclear aggregate formation in HD150QG mice at an advanced stage. (a) Frozen sections from 32-week-old transgenic mice were processed for either immunofluorescence (i–iii) or immunohistochemical staining with anti-ubiquitin (iv–vi). A CY3-labeled (red) secondary antibody was used to detect ubiquitin and the images of EGFP aggregates and ubiquitinated aggregates were then merged. Yellow arrows indicate ubiquitin-positive nuclear aggregates that still retained weak EGFP fluorescence, while red arrows indicate ubiquitin-positive nuclear aggregates that totally lost EGFP fluorescence. Scale bars, 20 μm. The white arrowheads point to cytoplasmic aggregates and the white arrows indicate nuclear aggregates. Electron microscopic examination of brain sections from transgenic mice (vii, hippocampus area; viii, cerebral cortex area) demonstrated the presence of dark neurons particularly in the hippocampus (arrow) and nuclear aggregates in the cerebral cortex (arrow). Scale bar, 10 and 5 μm in (vii and viii), respectively. (b) Nuclear accumulation of the transgene product. Brain samples from 5-week-old (5W) and 33-week-old (33W) HD150QG mice were subjected to subcellular fractionation as described in Materials and methods. The transgene products were detected by anti-GFP or 1C2 antibodies in both total homogenates (Homo) and nuclei (Nuc). In the brains of 33-week-old transgenic mice, the amount of nuclear-accumulated transgene products or their cleavage products was reduced due to aggregation. β-Tubulin and lamin B were used as markers for cytoplasmic and nuclear protein, respectively. W: wildtype, T: transgenic (c) Evidence for proteolytic processing of the transgene products. Frozen brain sections from 32-week-old HD150QG mice were immunohistochemically stained using either N-terminal huntingtin (Htt) antibody (i) or GFP polyclonal antibody (ii). Arrows indicate nuclear aggregates. Scale bar, 20 μm for both (i and ii).

high-density oligonucleotide array (GeneChip). GeneChip profiling was performed in the cerebrum of HD190QG and R6/2 mice and their littermate controls. Supplementary Table S2 summarizes data on the differentially expressed genes identified in all comparisons. We found that the expression levels of 148 genes were altered in HD190QG mice when compared with littermate controls. The number of genes showing decreased or increased expression in the cerebrum of transgenic mice was 100 and 48, respectively. A large fraction of the altered genes in HD190QG was comparable with those in the cerebrum of R6/2 mice (supplementary Table S2).

Decreased expression of hypothalamic neuropeptide mRNAs in HD190QG mice

Although many altered genes have previously been reported in the striatum of R6/2 mice (Luthi-Carter *et al.* 2000), we found additional genes with altered expression in this analysis (see supplementary Tables S2 and S3). In addition to the dopamine- and cAMP-regulated phosphoprotein, Mr 32 000 (DARPP-32) and enkephalin, which are predominantly expressed in the striatum and were reported as down-regulated in R6/2 mice (Luthi-Carter *et al.* 2000), expression of six hypothalamic neuropeptides was significantly decreased in the brains of 8-week-old HD190QG mice. Oxytocin and vasopressin mRNAs, which are abundantly expressed in the hypothalamus, were down-regulated in HD190QG brains. In addition, we also found, through GeneChip screening, that the expression of an Expressed Sequence Tag (EST), AI322575, was significantly decreased in HD190QG mice (supplementary Table S3). We predicted the coding region of the EST using several bioinformatical tools such as EST and mouse genome databases. AI322575 is

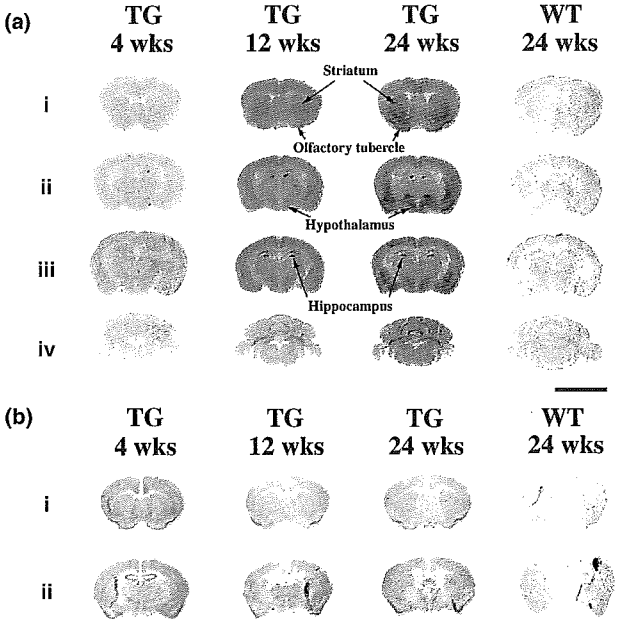

Fig. 4 Distribution of EGFP-positive aggregates in HD190QG mice. (a) Macroscopic analysis of the expanded polyglutamine (polyQ)-EGFP aggregates by a fluorescent imager. The frozen coronal brain sections were from 4–24-week-old HD190QG mice. Sections were directly observed using a fluorescent imager. Different slices of cortex (i–iii) and cerebellum (iv). (b) Widespread expression of transgene in HD190QG mice. *In situ* hybridization using an EGFP probe in slices (i and ii) indicates that expanded polyQ-EGFP mRNA was observed in all brain regions of HD190QG [transgenic (TG)] of different ages (4–24 weeks). In contrast, positive signals were not observed in littermate control brains [wild type (WT)]. Scale bar, 5 mm.

a part of cDNA encoding the neuropeptide CART (Adams *et al.* 1999), which is expressed in several hypothalamic regions and has been shown to be involved in the central control of food intake (Kong *et al.* 2003). Furthermore, expression of hypothalamic peptides, such as neuropeptide Y, prepro-thyroid-stimulating hormone-releasing hormone and prepro-somatostatin, was suggested to be decreased in HD190QG mice by GeneChip analysis.

We then confirmed the altered gene expression in the cerebrum by TaqMan RT-PCR assay. As shown in Figs 5(a and b), the levels of DARPP-32 and enkephalin were decreased in HD190QG and R6/2 mice. In contrast, the expression of prepro-tachykinin A mRNA, which is expressed in medium spiny neurons, was unchanged between the control and HD190QG brains (Fig. 5c).

The expression of six hypothalamic peptides of oxytocin, vasopressin, CART, neuropeptide Y, prepro-thyroid-stimulating hormone-releasing hormone and prepro-somatostatin mRNAs was decreased in HD190QG brains (Figs 5d–i). Similar results were also obtained in R6/2 mice (Fig. 5).

Distribution of the EGFP fluorescence in the HD190QG mice corresponds to the regions where dopamine- and cAMP-regulated phosphoprotein, Mr 32 000, oxytocin, vasopressin and cocaine-amphetamine-regulated transcript mRNAs are down-regulated

We investigated the distribution of DARPP-32 and oxytocin, vasopressin and CART mRNA in brains of 12- and 24-week-old HD190QG mice and their littermate controls by *in situ* hybridization. The DARPP-32 mRNA was expressed at high levels in the striatum, layer V of the cerebral cortex and the olfactory tubercle in the littermate controls of HD190HD mice (Fig. 6a). In contrast, the level of DARPP-32 expression was decreased at 12 and 24 weeks in HD190QG mice.

Oxytocin, vasopressin and CART mRNAs were expressed prominently in the hypothalamus of control brains (Fig. 6b). Both oxytocin and vasopressin mRNAs were expressed in

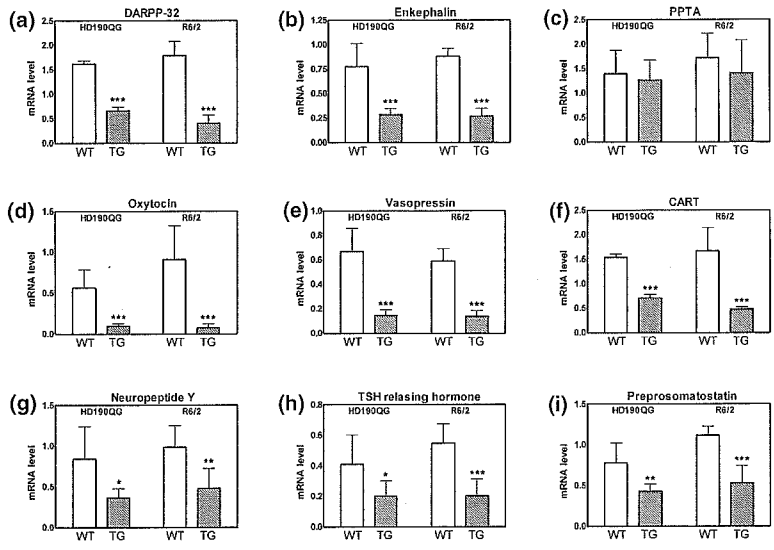

Fig. 5 TaqMan RT-PCR analysis of differentially expressed genes in 8-week-old HD190QG and R6/2 mice. TaqMan RT-PCR analysis was carried out in wild-type (WT) vs. HD190QG and R6/2 mice as described in Materials and methods. Values are given as mean ± SD ($n = 4$). (a) Dopamine- and cAMP-regulated phosphoprotein, Mr 32 000 (DARPP-32); (b) enkephalin; (c) prepro-tachykinin A (PPTA); (d) oxytocin; (e) vasopressin; (f) cocaine-amphetamine-regulated transcript (CART); (g) neuropeptide Y; (h) prepro-thyroid-stimulating hormone (TSH)-releasing hormone; (i) prepro-somatostatin. $^{*}p < 0.05$; $^{**}p < 0.01$; $^{***}p < 0.001$. TG, transgenic.

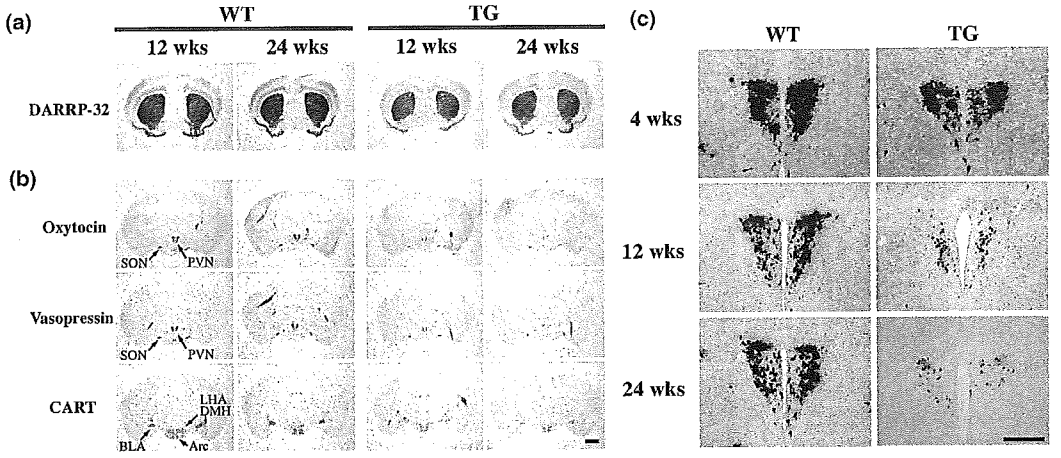

Fig. 6 *In situ* hybridization of genes differentially expressed in wild-type (WT) and HD190QG [transgenic (TG)] mice. Representative patterns of hybridization signals for dopamine- and cAMP-regulated phosphoprotein, Mr 32 000 (DARPP-32) in the striatum (a) and oxytocin, vasopressin and cocaine-amphetamine-regulated transcript (CART) mRNAs in the hypothalamus (b) were presented. (a) DARPP-32 mRNA was expressed at high levels in the striatum, cerebral cortex layer V and olfactory tubercle in WT mouse brain. mRNA expression was significantly decreased in TG mouse brain. (b) Both oxytocin and vasopressin mRNAs were expressed in supraoptic nuclei (SON) and paraventricular nuclei (PVN). CART mRNA was abundant in dorsomedial nuclei of the hypothalamus (DMH) and ventromedial nuclei of the hypothalamus. The levels of these mRNAs were significantly decreased in TG. Scale bar, 1 mm. (c) Decreased expression of oxytocin mRNA was observed in the hypothalamus of HD190QG mouse brain. A significant decrease in oxytocin mRNA was observed in the hypothalamus of 12- and 24-week-old HD190QG mice. Scale bar, 300 μm. Arc, arcuate nuclei; BLA, basolateral nuclei of the amygdala; LHA, lateral hypothalmic area.

supraoptic nuclei and paraventricular nuclei, whereas CART mRNA was abundant in the lateral hypothalamic area, dorsomedial nuclei of the hypothalamus, basolateral nuclei of the amygdala and arcuate nuclei. The levels of these mRNAs were largely decreased in HD190QG mice (Fig. 6b).

Interestingly, the distribution of EGFP-positive cytoplasmic aggregates of expanded polyQ-EGFP fusion protein in HD190QG mice corresponds to the regions where DARPP-32 and oxytocin, vasopressin and CART mRNAs were down-regulated (Figs 4a and 6).

We next checked how hypothalamic neuropeptide mRNAs decreased in HD190QG. We examined the levels of oxytocin mRNA by *in situ* hybridization. As shown in Fig. 6(c), the mRNA levels of oxytocin did not change at 4 weeks of age in HD190QG mice. In contrast, oxytocin mRNA is markedly decreased at 12 and 24 weeks of age, with an almost constant decrease observed in both cases.

We further studied the relationship between down-regulated gene expression, transgene expression and aggregate formation in the hypothalamus of HD190QG and littermate controls (Fig. 7). Although oxytocin mRNA was significantly decreased in HD190QG mice, there was no correlation between the altered gene expression and transgene expression as analysed by *in situ* hybridization using an EGFP probe (Fig. 7a). However, we found that many anti-N-terminal huntingtin-immunoreactive aggregates were observed in the paraventricular nuclei of the hypothalamus of HD190QG, where the expression of oxytocin mRNA was down-regulated. Similar results were also obtained for CART in the lateral hypothalamic area and dorsomedial nuclei of the hypothalamus (Fig. 7b). Thus, there is a correlation between aggregate formation and decreases in specific gene expression in the hypothalamus.

Decreased gene expression of oxytocin without a significant decrease in hypothalamic neurons in HD190QG mice

Scoring oxytocin-expressing neurons in the hypothalamus of 24-week-old HD190QG clearly indicated that oxytocin-positive neurons were markedly decreased in HD190QG (Fig. 8a). We then counted the neuronal nuclei in the striatum using an antibody which recognizes NeuN (Azzouz *et al.* 2000). Quantification of neuronal nuclei in the hypothalamus using NeuN indicated that hypothalamic neurons were not lost in HD190QG mice at 24 weeks (Fig. 8b).

Discussion

EGFP is widely used in many studies of HD for labeling mammalian cells in culture or in multicellular organisms but, as yet, has not been utilized for disease model mice. To study aggregate formation of expanded polyQ in the brain, we have established transgenic mouse lines expressing expanded polyQ as a fusion with EGFP under the control of the huntingtin promoter. By using these mice in combination

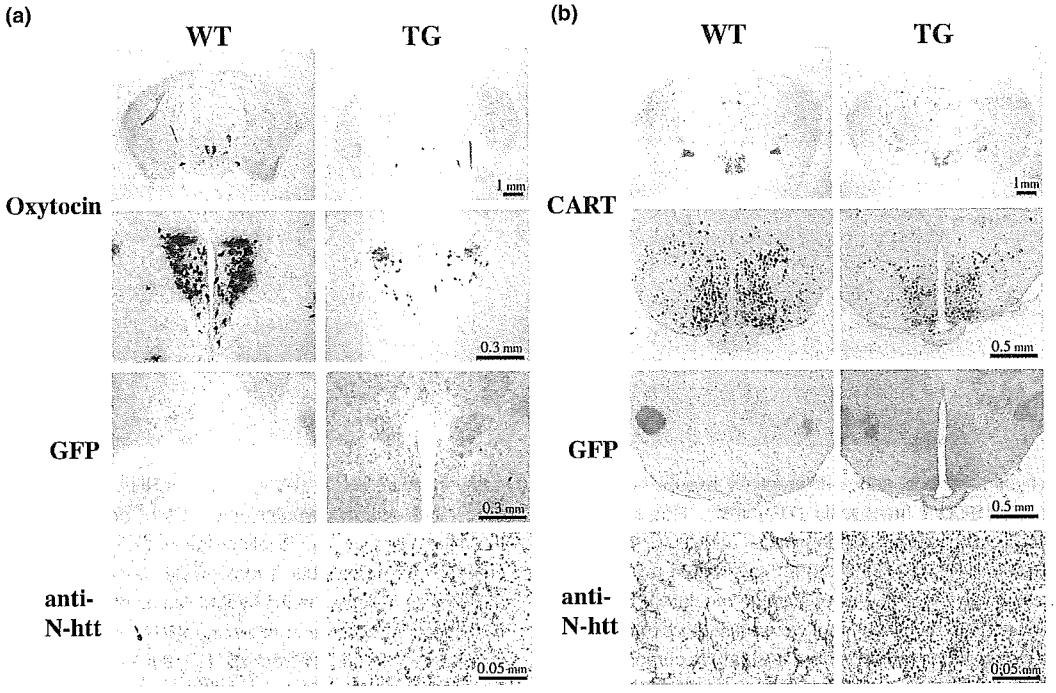

Fig. 7 The relationship between altered gene expression, transgene expression and aggregate formation in the hypothalamus. Serial sections (20 μm thick) were prepared from 24-week-old wild-type (WT) or HD190QG [transgenic (TG)] mice and processed for *in situ* hybridization and immunohistochemistry. Coronal sections were prepared according to the regions of Bregma −0.94 mm (a; for oxytocin mRNA) and −2.18 mm [b; for cocaine-amphetamine-regulated transcript (CART) mRNA expression] based on the atlas of Franklin and Paxinos (1997). Higher magnification views of sections corresponding to the hypothalamus are shown below. Transgene expression assessed using an EGFP probe are also shown (shown as GFP). The sections were immunohistochemically stained using N-terminal huntingtin antibody (anti-N-htt).

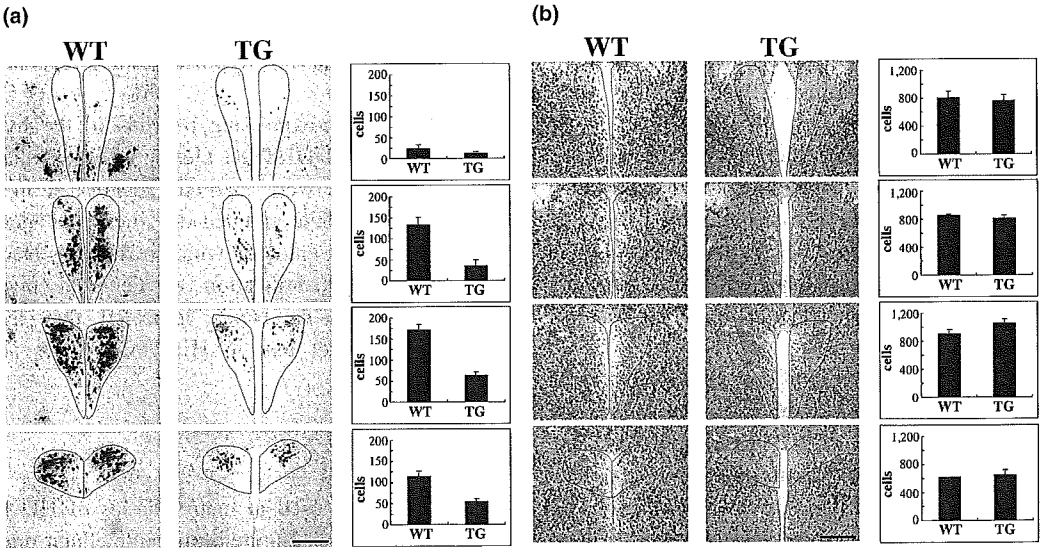

Fig. 8 Counting of oxytocin mRNA-expressing neurons and neuron-specific nuclear protein (NeuN)-positive neurons in the hypothalamus. Serial sections (20 μm thick) were prepared from 24-week-old wild-type (WT) or HD190QG [transgenic (TG)] mice and processed for *in situ* hybridization (a) or immunohistochemistry using NeuN (b). The number of oxytocin mRNA-positive or NeuN-positive cells in the areas enclosed within the red lines were counted. Images show every 200-μm serial section. We analysed three WT and three TG mice. Values are given as mean ± SD.

with confocal microscopy and fluorescent imaging, we found that the transgene product forms aggregates in the hypothalamus as well as in the striatum and hippocampus.

These mice could be useful for further HD studies. Firstly, striatal and hippocampal neurons of our transgenic mice can be maintained in culture and aggregate formation can be observed in living cells by fluorescence microscopy. Secondly, using a fluorescence-activated cell sorter we can purify the polyQ-EGFP aggregates in both cytoplasm and nuclei in our mouse models. Indeed, we have purified the cytoplasmic aggregates from neuro2a cells expressing expanded polyQ-EGFP, with the aid of a fluorescence-activated cell sorter, and identified several aggregate-interacting proteins (Mitsui *et al.* 2002). Finally, molecules that are able to suppress polyQ aggregation are now considered potential therapeutic molecules (Ferrante *et al.* 2003; Hockly *et al.* 2003; Sanchez *et al.* 2003; Tanaka *et al.* 2004). Our EGFP mouse model, in combination with a fluorescent imager, could provide a simple and sensitive tool for *in vivo* testing of potentially therapeutic molecules for inhibiting aggregate formation.

R6/2 and our HD190QG mice (transgene, an EGFP-tagged huntingtin exon 1) display progressive neurological phenotypes which are very similar to those seen in the human disease. There is a marked difference in survival between our expanded polyQ-EGFP transgenic and R6/2 mice. This might be due to the presence of EGFP in addition to the expanded polyQ, which stabilizes the molecule and reduces the formation of polyQ aggregates *in vivo*.

The cytoplasmic and nuclear aggregation of expanded polyQ-EGFP fusion proteins were observed in striatal and hippocampal neurons in younger mice and increased progressively with age. In older transgenic mice, the ubiquitin-positive nuclear aggregates lost EGFP fluorescence although they still had EGFP immunoreactivity. The loss of fluorescence in nuclear aggregates does not appear to be due to age as the cytoplasmic aggregates increase progressively with increased age. It is also unlikely to be due to the association of nuclear proteins, as reported earlier (Perez *et al.* 1998; Boutell *et al.* 1999; Shimohata *et al.* 2000). Our results suggest that proteolytic processing, particularly in the nucleus, is involved in this loss of fluorescence. Although we do not know the identity of the protease or the specific cleavage site, it is possible that proteasomes may be involved in this proteolytic processing as proteasomes associate with the nuclear aggregates and have been shown to remove aggregates (Yamamoto *et al.* 2000; Martin-Aparicio *et al.* 2001).

Luthi-Carter *et al.* (2000) have identified genes that were aberrantly expressed in the striatum of R6/2 mice using GeneChip analysis. Their experiments showed a general down-regulation of striatal signaling genes and up-regulation of genes indicative of stress and inflammation. In this report we compared differentially expressed genes between HD190QG and control mice in the cerebrum and found that expression of hypothalamic peptide mRNAs, such as oxytocin, vasopressin and CART, was reduced in HD190QG mice in addition to the already reported altered genes, indicating the region-specific dysregulation of gene expression in the hypothalamus as well as the striatum in the brains of HD190QG mice.

The polyQ-EGFP transgene was widely expressed in transgenic mouse brain (Fig. 4b), which is consistent with endogenous huntingtin (Gutekunst *et al.* 1995; Landwehrmeyer *et al.* 1995). However, EGFP fluorescence in brain sections was more pronounced in the striatum, hippocampus and hypothalamus in 12–24-week-old HD190QG mice (Fig. 4a), indicating that there is no direct correlation between transgene expression and aggregate formation. The distribution of aggregates is nearly correlated with the down-regulated expression of specific genes found in the striatum and hypothalamus in HD190QG mice. Thus, the presence of aggregates may lead to decreased levels of specific mRNAs in both the striatum and hypothalamus in our HD transgenic mice. As neurons accumulating expanded polyQ-EGFP did not selectively express high levels of the expanded polyQ mRNA in our mice (see Fig. 4b), the region-specific accumulation of expanded polyQ-EGFP does not result from local overexpression of the transgene.

Huntington disease is associated with weight loss in patients from early stages of the disease (Djousse *et al.* 2002). The complex neural circuits maintaining constancy of weight consist of many groups of neurons in the hypothalamus and other brain regions (Kalra *et al.* 1999). Selective neuronal loss in the hypothalamic lateral nucleus in HD patients has been demonstrated (Kremer *et al.* 1990, 1991) and atrophy of hypothalamic nuclei was confirmed by magnetic resonance imaging (Kassubek *et al.* 2004). Recently, hypothalamic degeneration in HD transgenic mice has been described (Li *et al.* 2003; Petersen *et al.* 2005). In our study, the gene expression in distinct areas in the hypothalamus was analysed by *in situ* hybridization and by counting neuronal cell numbers. Clear differences in gene expression were observed in this area, suggesting that transcriptional dysregulation occurs in each diseased neuron. In addition, our data reveal a down-regulation of mRNAs for a number of hypothalamic peptides that are known to be involved in feeding behavior and energy homeostasis. Different types of neurodegeneration in HD may lead to a variety of neurological symptoms. Dysfunction and degeneration of neurons in the striatum could be associated with motor and behavioral abnormalities. Dysregulated gene expression in the hypothalamus may lead to wasting and body weight loss. Our present results reveal consistent hypothalamic lesions in different HD mouse models.

Acknowledgements

We are grateful to Prof.M. MacDonald (Massachusetts General Hospital) for the HD promoter. We thank Mr K. Fukumoto (RIKEN

Brain Science Institute Research Resource Center) for GeneChip analysis. We also thank Drs M. Tateno, M. Tanaka and S. Itohara (RIKEN Brain Science Institute) for valuable advice on determining copy number of the transgene and Dr J. Doumanis (our laboratory) for critical reading of this manuscript. This work was supported in part by a Grant-in-Aid from the Ministry of Health, Labor and Welfare and from the Ministry of Education, Culture, Sports, Science and Technology, Japan.

References

Adams L. D., Gong W., Vechia S. D., Hunter R. G. and Kuhar M. J. (1999) CART: from gene to function. *Brain Res.* **848**, 137–140.

Azzouz M., Hottinger A., Paterna J. C., Zurn A. D., Aebischer P. and Bueler H. (2000) Increased motoneuron survival and improved neuromuscular function in transgenic ALS mice after intraspinal injection of an adeno-associated virus encoding Bcl-2. *Hum. Mol. Genet.* **9**, 803–811.

Boutell J. M., Thomas P., Neal J. W., Weston V. J., Duce J., Harper P. S. and Jones A. L. (1999) Aberrant interactions of transcriptional repressor proteins with the Huntington's disease gene product, huntingtin. *Hum. Mol. Genet.* **8**, 1647–1655.

Davies S. W., Turmaine M., Cozens B. A., DiFiglia M., Sharp A. H., Ross C. A., Scherzinger E., Wanker E. E., Mangiarini L. and Bates G. P. (1997) Formation of neuronal intranuclear inclusions underlies the neurological dysfunction in mice transgenic for the HD mutation. *Cell* **90**, 537–548.

DiFiglia M., Sapp E., Chase K. O., Davies S. W., Bates G. P., Vonsattel J. P. and Aronin N. (1997) Aggregation of huntingtin in neuronal intranuclear inclusions and dystrophic neurites in brain. *Science* **277**, 1990–1993.

Djousse L., Knowlton B., Cupples L. A., Marder K., Shoulson I. and Myers R. H. (2002) Weight loss in early stage of Huntington's disease. *Neurology* **59**, 1325–1330.

Ferrante R. J., Kubilus J. K., Lee J. *et al.* (2003) Histone deacetylase inhibition by sodium butyrate chemotherapy ameliorates the neurodegenerative phenotype in Huntington's disease mice. *J. Neurosci.* **23**, 9418–9427.

Franklin K. B. J. and Paxinos G. (1997) *The Mouse Brain in Stereotaxic Coordinates*. Academic Press, San Diego.

Gingrich J. C., Davis D. R. and Nguyen Q. (2000) Multiplex detection and quantitation of proteins on western blots using fluorescent probes. *Biotechniques* **29**, 636–642.

Gutekunst C. A., Levey A. I., Heilman C. J., Whaley W. L., Yi H., Nash N. R., Rees H. D., Madden J. J. and Hersch S. M. (1995) Identification and localization of huntingtin in brain and human lymphoblastoid cell lines with anti-fusion protein antibodies. *Proc. Natl Acad. Sci. USA* **92**, 8710–8714.

Harper A. (1991) *Huntington's Disease*. W.B. Saunders, London.

Hockly E., Richon V. M., Woodman B. *et al.* (2003) Suberoylanilide hydroxamic acid, a histone deacetylase inhibitor, ameliorates motor deficits in a mouse model of Huntington's disease. *Proc. Natl Acad. Sci. USA* **100**, 2041–2046.

Hodgson J. G., Agopyan N., Gutekunst C. A. *et al.* (1999) A YAC mouse model for Huntington's disease with full-length mutant huntingtin, cytoplasmic toxicity, and selective striatal neurodegeneration. *Neuron* **23**, 181–192.

Huntington's Disease Collaborative Research Group (1993) A novel gene containing a trinucleotide repeat that is expanded and unstable on Huntington's disease chromosomes. *Cell* **72**, 971–983.

Ishiguro H., Yamada K., Sawada H. *et al.* (2001) Age-dependent and tissue-specific CAG repeat instability occurs in mouse knock-in for a mutant Huntington's disease gene. *J. Neurosci. Res.* **65**, 289–297.

Kalra S. P., Dube M. G., Pu S., Xu B., Horvath T. L. and Kalra P. S. (1999) Interacting appetite-regulating pathways in the hypothalamic regulation of body weight. *Endocr. Rev.* **20**, 68–100.

Kassubek J., Juengling F. D., Kioschies T. *et al.* (2004) Topography of cerebral atrophy in early Huntington's disease: a voxel based morphometric MRI study. *J. Neurol. Neurosurg. Psychiat.* **75**, 213–220.

Klement I. A., Skinner P. J., Kaytor M. D., Yi H., Hersch S. M., Clark H. B., Zoghbi H. Y. and Orr H. T. (1998) Ataxin-1 nuclear localization and aggregation: role in polyglutamine-induced disease in SCA1 transgenic mice. *Cell* **95**, 41–53.

Kong W. M., Stanley S., Gardiner J., Abbott C., Murphy K., Seth A., Connoley I., Ghatei M., Stephens D. and Bloom S. (2003) A role for arcuate cocaine and amphetamine-regulated transcript in hyperphagia, thermogenesis, and cold adaptation. *Faseb J.* **17**, 1688–1690.

Kremer H. P., Roos R. A., Dingjan G., Marani E. and Bots G. T. (1990) Atrophy of the hypothalamic lateral tuberal nucleus in Huntington's disease. *J. Neuropathol. Exp. Neurol.* **49**, 371–382.

Kremer H. P., Roos R. A., Dingjan G. M., Bots G. T., Bruyn G. W. and Hofman M. A. (1991) The hypothalamic lateral tuberal nucleus and the characteristics of neuronal loss in Huntington's disease. *Neurosci. Lett.* **132**, 101–104.

Landwehrmeyer G. B., McNeil S. M., Dure L. S. T. *et al.* (1995) Huntington's disease gene: regional and cellular expression in brain of normal and affected individuals. *Ann. Neurol.* **37**, 218–230.

Li H., Li S. H., Johnston H., Shelbourne P. F. and Li X. J. (2000) Amino-terminal fragments of mutant huntingtin show selective accumulation in striatal neurons and synaptic toxicity. *Nat. Genet.* **25**, 385–389.

Li S. H., Yu Z. X., Li C. L., Nguyen H. P., Zhou Y. X., Deng C. and Li X. J. (2003) Lack of huntingtin-associated protein-1 causes neuronal death resembling hypothalamic degeneration in Huntington's disease. *J. Neurosci.* **23**, 6956–6964.

Lin C. H., Tallaksen-Greene S., Chien W. M., Cearley J. A., Jackson W. S., Crouse A. B., Ren S., Li X. J., Albin R. L. and Detloff P. J. (2001) Neurological abnormalities in a knock-in mouse model of Huntington's disease. *Hum. Mol. Genet.* **10**, 137–144.

Luthi-Carter R., Strand A., Peters N. L. *et al.* (2000) Decreased expression of striatal signaling genes in a mouse model of Huntington's disease. *Hum. Mol. Genet.* **9**, 1259–1271.

Mangiarini L., Sathasivam K., Seller M. *et al.* (1996) Exon 1 of the HD gene with an expanded CAG repeat is sufficient to cause a progressive neurological phenotype in transgenic mice. *Cell* **87**, 493–506.

Martin-Aparicio E., Yamamoto A., Hernandez F., Hen R., Avila J. and Lucas J. J. (2001) Proteasomal-dependent aggregate reversal and absence of cell death in a conditional mouse model of Huntington's disease. *J. Neurosci.* **21**, 8772–8781.

Meade C. A., Deng Y. P., Fusco F. R., Del Mar N., Hersch S., Goldowitz D. and Reiner A. (2002) Cellular localization and development of neuronal intranuclear inclusions in striatal and cortical neurons in R6/2 transgenic mice. *J. Comp. Neurol.* **449**, 241–269.

Mitsui K., Nakayama H., Akagi T., Nekooki M., Ohtawa K., Takio K., Hashikawa T. and Nukina N. (2002) Purification of polyglutamine aggregates and identification of elongation factor-1alpha and heat shock protein 84 as aggregate-interacting proteins. *J. Neurosci.* **22**, 9267–9277.

Morton A. J., Lagan M. A., Skepper J. N. and Dunnett S. B. (2000) Progressive formation of inclusions in the striatum and hippocampus of mice transgenic for the human Huntington's disease mutation. *J. Neurocytol.* **29**, 679–702.

Nagai T., Aruga J., Takada S., Gunther T., Sporle R., Schughart K. and Mikoshiba K. (1997) The expression of the mouse Zic1, Zic2, and

Zic3 gene suggests an essential role for Zic genes in body pattern formation. *Dev. Biol.* **182**, 299–313.

Ona V. O., Li M., Vonsattel J. P. *et al.* (1999) Inhibition of caspase-1 slows disease progression in a mouse model of Huntington's disease. *Nature* **399**, 263–267.

Paulson H. L. (1999) Protein fate in neurodegenerative proteinopathies: polyglutamine diseases join the (mis)fold. *Am. J. Hum. Genet.* **64**, 339–345.

Perez M. K., Paulson H. L., Pendse S. J., Saionz S. J., Bonini N. M. and Pittman R. N. (1998) Recruitment and the role of nuclear localization in polyglutamine-mediated aggregation. *J. Cell Biol.* **143**, 1457–1470.

Petersen A., Gil J., Maat-Schieman M. L. *et al.* (2005) Orexin loss in Huntington's disease. *Hum. Mol. Genet.* **14**, 39–47.

Reddy P. H., Williams M., Charles V., Garrett L., Pike-Buchanan L., Whetsell W. O. Jr, Miller G. and Tagle D. A. (1998) Behavioural abnormalities and selective neuronal loss in HD transgenic mice expressing mutated full-length HD cDNA. *Nat. Genet.* **20**, 198–202.

Sanchez I., Mahlke C. and Yuan J. (2003) Pivotal role of oligomerization in expanded polyglutamine neurodegenerative disorders. *Nature* **421**, 373–379.

Saudou F., Finkbeiner S., Devys D. and Greenberg M. E. (1998) Huntingtin acts in the nucleus to induce apoptosis but death does not correlate with the formation of intranuclear inclusions. *Cell* **95**, 55–66.

Schilling G., Becher M. W., Sharp A. H. *et al.* (1999) Intranuclear inclusions and neuritic aggregates in transgenic mice expressing a mutant N-terminal fragment of huntingtin. *Hum. Mol. Genet.* **8**, 397–407.

Sherman M. Y. and Goldberg A. L. (2001) Cellular defenses against unfolded proteins: a cell biologist thinks about neurodegenerative diseases. *Neuron* **29**, 15–32.

Shimohata T., Nakajima T., Yamada M. *et al.* (2000) Expanded polyglutamine stretches interact with TAFII130, interfering with CREB-dependent transcription. *Nat. Genet.* **26**, 29–36.

Tanaka M., Machida Y., Niu S., Ikeda T., Jana N. R., Doi H., Kurosawa M., Nekooki M. and Nukina N. (2004) Trehalose alleviates polyglutamine-mediated pathology in a mouse model of Huntington disease. *Nat. Med.* **10**, 148–154.

Tateno M., Sadakata H., Tanaka M. *et al.* (2004) Calcium-permeable AMPA receptors promote misfolding of mutant SOD1 protein and development of amyotrophic lateral sclerosis in a transgenic mouse model. *Hum. Mol. Genet.* **13**, 2183–2196.

Trottier Y., Lutz Y., Stevanin G. *et al.* (1995) Polyglutamine expansion as a pathological epitope in Huntington's disease and four dominant cerebellar ataxias. *Nature* **378**, 403–406.

Turmaine M., Raza A., Mahal A., Mangiarini L., Bates G. P. and Davies S. W. (2000) Nonapoptotic neurodegeneration in a transgenic mouse model of Huntington's disease. *Proc. Natl Acad. Sci. USA* **97**, 8093–8097.

Usdin M. T., Shelbourne P. F., Myers R. M. and Madison D. V. (1999) Impaired synaptic plasticity in mice carrying the Huntington's disease mutation. *Hum. Mol. Genet.* **8**, 839–846.

Vonsattel J. P. and DiFiglia M. (1998) Huntington disease. *J. Neuropathol. Exp. Neurol.* **57**, 369–384.

Wheeler V. C., White J. K., Gutekunst C. A. *et al.* (2000) Long glutamine tracts cause nuclear localization of a novel form of huntingtin in medium spiny striatal neurons in HdhQ92 and HdhQ111 knock-in mice. *Hum. Mol. Genet.* **9**, 503–513.

Yamamoto A., Lucas J. J. and Hen R. (2000) Reversal of neuropathology and motor dysfunction in a conditional model of Huntington's disease. *Cell* **101**, 57–66.

Zoghbi H. Y. and Orr H. T. (2000) Glutamine repeats and neurodegeneration. *Annu. Rev. Neurosci.* **23**, 217–247.

NEUROLOGY

Progression of the olivopontocerebellar form of adrenoleukodystrophy as shown by MRI

S. Suda, Y. Komaba, T. Kumagai, M. Yamazaki, T. Katsumata, T. Kamiya and Y. Katayama

Neurology 2006;66;144-145
DOI: 10.1212/01.wnl.0000191329.34585.15

This information is current as of January 10, 2006

The online version of this article, along with updated information and services, is located on the World Wide Web at:
http://www.neurology.org/cgi/content/full/66/1/144

Neurology is the official journal of AAN Enterprises, Inc. A bi-monthly publication, it has been published continuously since 1951. Copyright © 2006 by AAN Enterprises, Inc. All rights reserved. Print ISSN: 0028-3878. Online ISSN: 1526-632X.

AMERICAN ACADEMY OF NEUROLOGY

Downloaded from www.neurology.org by MINEO YAMAZAKI on January 10, 2006

Within a few days, she had reverse "sniffing" when tired and said, "Mom, I don't mean to do this." She also had stereotypical wiping of her nose with the left hand. The following day, she had brief nasal flaring and grunting in addition to arm abduction and head protrusion. The medication was reviewed and found to contain 10 mg of mepyramine maleate in addition to 50 mg of guaifenesin per dose. The movements improved within a few days of stopping the medication. Of note, the child had no difficulty the previous month when given an over-the-counter medication containing guaifenesin plus pseudoephedrine.

Discussion. Cetirizine is an over-the-counter highly selective histamine H1-receptor antagonist.[1] It is one of only two second-generation antihistamines approved by the Food and Drug Administration for children younger than 5 years old.[2] The large size, lipophobic nature, and greater peripheral H1-receptor affinity are thought to minimize CNS penetration and central side effects. However, one PET study of cetirizine shows approximately 30% cerebral cortex H1-receptor binding.[1] Cetirizine is a carboxylated metabolite of hydroxyzine,[1] a first-generation piperazine H1-receptor antagonist.[3] Piperazines have central D2-dopaminergic blocking properties and are used as antipsychotic agents.[3] We postulate that as a piperazine derivative, cetirizine has dopamine receptor blocking properties in susceptible individuals and caused the dystonic movements in our case.

There are cases of reversible cetirizine-induced oculogyric crisis previously reported in the pediatric literature.[4] Furthermore, a 13-year-old girl developed dystonic movements after 2 months of treatment with hydroxyzine.[5] IV cimetidine, a histamine H2-receptor antagonist, is associated with acute dystonic reaction in a 39-year-old woman with masseter spasm and oculogyric crisis who had a history of a similar reaction following IV prochlorperazine.[6]

As this child tolerated guaifenesin in other formulations, we believe mepyramine was the component triggering recurrence of her symptoms. Mepyramine, an ethylenediamine, is a first-generation H1 antagonist with CNS penetration.[3] Although mepyramine is not known to interact with the dopamine system, histamine is reported to in some human studies. This may represent a physiologic explanation for our observation, although animal studies reveal contradictory evidence.[7]

This young girl developed repetitive, stereotyped, involuntary dystonic movements after nearly 3 weeks on daily cetirizine syrup given at the recommended dose. She developed similar movements within a few days of mepyramine exposure. These movements likely represent dystonic tics. There was no sustained, fixed posturing.

From the Division of Neurology (A.R.) and Department of Pediatrics (K.B.), University of Saskatchewan, Saskatoon, Canada.

Disclosure: The authors report no conflicts of interest.

Received July 24, 2005. Accepted in final form October 4, 2005.

Address correspondence and reprint requests to Dr. A. Rajput, Division of Neurology, University of Saskatchewan, 103 Hospital Dr., Saskatoon, SK S7N 0W8, Canada; e-mail: rajputa@sask.usask.ca

Copyright © 2006 by AAN Enterprises, Inc.

References

1. Curran MP, Scott LJ, Perry CM. Cetirizine: a review of its use in allergic disorders. Drugs 2004;64:523–561.
2. Ng KH, Chong D, Wong CK, et al. Central nervous system side effects of first- and second-generation antihistamines in school children with perennial allergic rhinitis: a randomized, double-blind, placebo-controlled comparative study. Pediatrics 2004;113:116–121.
3. Hardman JG, Limbird LE, Molinoff PB, Ruddon RW, Goodman Gilman A, eds. Goodman & Gilman's the pharmacological basis of therapeutics. 9th ed. New York: McGraw-Hill, 1996.
4. Fraunfelder FW, Fraunfelder FT. Oculogyric crisis in patients taking cetirizine. Am J Ophthalmol 2004;137:355–357.
5. Sandyk R. Alpha-melanocyte-stimulating hormone: possible role in the pathophysiology of acute drug-induced dystonia. Int J Neurosci 1990;53: 241–242.
6. Peiris RS, Peckler BF. Cimetidine-induced dystonic reaction. J Emerg Med 2001;21:27–29.
7. Korotkova TM, Haas HL, Brown RE. Histamine excites GABAergic cells in the rat substantia nigra and ventral tegmental area in vitro. Neurosci Lett 2002;320:133–136.

Progression of the olivopontocerebellar form of adrenoleukodystrophy as shown by MRI

S. Suda, MD; Y. Komaba, MD; T. Kumagai, MD; M. Yamazaki, MD; T. Katsumata, MD; T. Kamiya, MD; and Y. Katayama, MD

Adrenoleukodystrophy (ALD) is an X-linked recessive disorder characterized by demyelination of the CNS, adrenal insufficiency, and increased blood concentrations of very long chain fatty acids (VLCFA).[1] The clinical phenotype of ALD is variable. The most common type of ALD is the childhood cerebral form, in which T2-weighted MRI of the brain typically shows areas of hyperintense signal in parieto-occipital white matter.[2] In contrast, the olivopontocerebellar form of ALD is an uncommon phenotype identified in 1982 in an ALD family pedigree where clinical features resembled those of spinocerebellar degeneration.[3] We report progression demonstrated by MRI in a patient whose olivopontocerebellar form of ALD included certain atypical lesions.

Case report. A 29-year-old man was hospitalized with progressive gait disturbance and dysarthria for 6 months. He had a history of Addison disease beginning 3 years previously, treated with dexamethasone. On admission, physical examination showed increased skin pigmentation. Neurologic examination disclosed cerebellar ataxia, exaggerated deep tendon reflexes, and pathologic reflexes in all extremities. No mental disorder, visual disturbance, sensory deficit, or sphincteric disturbance was present. Results of CSF examination were normal. A rapid adrenocorticotropic hormone stimulation test showed a greatly decreased response, suggesting adrenal insufficiency. T2-weighted MRI of the brain showed hyperintense areas in both dentate nuclei and red nuclei and in the pontine portion of the left corticospinal tract (figure, A to E). No lesions were demonstrated by MRI in cerebral white matter. Analysis of VLCFA in peripheral blood revealed marked elevation of C24:0/C22:0, C25:0/C22:0, and C26:0/C22:0 ratios. The patient was diagnosed with the olivopontocerebellar form of ALD. Despite the importance of information concerning genotype-phenotype correlation in this disorder, consent for ALD genetic testing was withheld by the patient. At 24 months from symptom onset, he had become bedridden because of progressive ataxia and spastic tetraplegia. He had severe dysphagia and dysarthria. T2-weighted MRI of the brain now showed additional hyperintense areas in the pontine portion of the right corticospinal tract, left thalamus, and in both medullary pyramids (figure, F to J). T2-weighted MRI of the spine showed mild atrophy of the cervicothoracic spinal cord without obvious abnormal intensities (figure, K and L). At 36 months after symptom onset, follow-up T2-weighted MRI of the brain showed progressive enlargement of lesions, and also new hyperintense areas bilaterally in the medial lemniscus of the brainstem, cerebral peduncle, and internal capsule and in the right thalamus (figure, M to Q). Follow-up T2-weighted MRI of the cervicothoracic spinal cord showed bilateral hyperintense areas in the lateral funiculi and posterior columns (figure, R and S).

Discussion. The olivopontocerebellar form accounts for only 1% to 2% of all cases of ALD. Few reported patients have been followed up by serial imaging to identify and characterize progression. We longitudinally studied MRI findings in our patient with this form of ALD. Progression of disease extent and distribution of lesions in the present patient was compared with previously reported brain MRI findings in patients with olivopontocerebellar ALD. These reported images disclosed demyelination of the cerebellum, cerebellar peduncles, and the corticospinal tracts from the medulla to internal capsule.[4,5] In the present patient, serial MRI indicated principal involvement of three functional types of tracts, with progression of disease as follows: 1) demyelination of the dentatorubrothalamic tract progressively extending from the red nuclei upward to the thalamus; 2) demyelination of the corticospinal tract extending downward from the pons to the spinal cord and upward to the internal capsule; and 3) progression of the posterior column-medial lemniscus lesion that was difficult to clarify by MRI. On the other hand, MRI of the spine reportedly has shown cord atrophy with no focal abnormality in intrinsic signal intensity.[6] In the present patient, bilateral involvement of

Downloaded from www.neurology.org by MINEO YAMAZAKI on January 10, 2006
Copyright © by AAN Enterprises, Inc. Unauthorized reproduction of this article is prohibited.

Figure. Serial MRI of the brain and cervicothoracic spinal cord, showing progression of demyelination. A to E: Images obtained 6 months after symptom onset. T2-weighted sequences show hyperintense areas in the dentate nuclei and red nuclei bilaterally, and in the left corticospinal tract at the level of the pons. F to L: Images obtained 24 months after symptom onset. T2-weighted sequences show new hyperintense areas in the right corticospinal tract at the level of the pons and left thalamus, and bilaterally in the medullary pyramids. T2-weighted imaging of the spinal cord at C5 and Th7 shows mild atrophy without obvious abnormal intensities. M to S: Images obtained 36 months after symptom onset. T2-weighted sequences show new hyperintense areas bilaterally in the brainstem medial lemniscus, cerebral peduncle, and internal capsule and in the right thalamus. T2-weighted image of the spinal cord shows bilateral hyperintense areas in the lateral funiculi and posterior columns.

posterior columns and lateral funiculi ultimately could be identified by serial MRI. Histologically, loss of axons and myelin has been observed in the corticospinal tract and in the posterior columns and medial lemniscus.[7] To our knowledge, the present report is the first account of ALD to show T2-weighted hyperintense areas in the spinal cord.

Early diagnosis of ALD phenotype, important for genetic counseling and choice of therapy, is usually based on MRI findings and clinical symptoms.

From the Second Department of Internal Medicine, Nippon Medical School, Tokyo, Japan.

Disclosure: The authors report no conflicts of interest.

Received May 16, 2005. Accepted in final form October 4, 2005.

Address correspondence and reprint requests to Dr. Satoshi Suda, Second Department of Internal Medicine, Nippon Medical School, 1-1-5 Sendagi, Bunkyo-ku 113-8602, Tokyo, Japan; e-mail: sachorin@gp-machiya.jp

Copyright © 2006 by AAN Enterprises, Inc.

References

1. Schaumburg HH, Powers JM, Raine CS, Richardson EP Jr. Adrenoleukodystrophy. A clinical and pathological study of 17 cases. Arch Neurol 1975;32:577–591.
2. Moser HW. Adrenoleukodystrophy: phenotype, genetics, pathogenesis and therapy. Brain 1997;120:1485–1508.
3. Marsden CD, Obeso JA, Lang AE. Adrenoleukomyeloneuropathy presenting as spinocerebellar degeneration. Neurology 1982;32:1031–1032.
4. Kusaka H, Imai T. Ataxic variant of adrenoleukodystrophy: MRI and CT findings. J Neurol 1992;239:307–310.
5. Kumar AJ, Kohler W, Kruse B, et al. MR findings in adult-onset adrenoleukodystrophy. AJNR Am J Neuroradiol 1995;16:1227–1237.
6. Snyder RD, King JN, Keck GM, Orrison WW. MR imaging of the spinal cord in 23 subjects with ALD-AMN complex. AJNR Am J Neuroradiol 1991;12:1095–1098.
7. Tateishi J, Sato Y, Suetsugu M, Takashiba T. Adrenoleukodystrophy with olivopontocerebellar atrophy-like lesions. Clin Neuropathol 1986;5:34–39.

Downloaded from www.neurology.org by MINEO YAMAZAKI on January 10, 2006
Copyright © by AAN Enterprises, Inc. Unauthorized reproduction of this article is prohibited.

Neuropathology 2005; **25**, 381–387

Workshop: Recent Advances in Motor Neuron Disease

Is motoneuronal cell death in amyotrophic lateral sclerosis apoptosis?

Mineo Yamazaki,[1,2] Eisaku Esumi[3] and Imaharu Nakano[4]

[1]Division of Neurology, 2nd Department of Internal Medicine, Nippon Medical School, [2]Department of Neuropathology, Tokyo Metropolitan Institute for Neuroscience, [3]Department of Neurology, Tokyo Tama Hospital, Tokyo and [4]Department of Neurology, Jichi Medical School, Tochigi, Japan

To clarify the controversy concerning whether the cell death of motor neurons in ALS is apoptosis, we investigated the expression of Apaf-1 and caspase-9 mRNA in spinal cord tissue obained at autopsy from patients with ALS and controls using RT-PCR; the presence of *in situ* nuclear DNA fragmentation in motor neurons by the TdT-mediated dUTP-biotin nick end-labeling (TUNEL) method; and immunocytochemical localization of Apaf-1 and caspase-3, which are known as promotors of apoptotic processes. Although Apaf-1 and caspase-9 mRNAs levels were increased in ALS, Apaf-1 immunoreactivity (IR) showed no significant difference between ALS and the control, and caspase-3 IR was not observed in ALS motoneurons, casting doubt on the notion that motor neurons in ALS undergo death by the classic apoptotic pathway. Although TUNEL-positive motor neurons were frequently observed in the anterior horn in ALS, these neurons always showed an atrophic cell body with a shrunken and pyknotic nucleus, indicating that they were at the terminal stage of degeneration. No apoptotic bodies were seen. These findings suggest that the mechanism of motor neuronal cell death in ALS might not be apoptosis, but some other as yet unidentified mechanism.

Key words: amyotrophic lateral sclerosis, Apaf-1, apoptosis, caspase, cell death, DNA fragmentation.

INTRODUCTION

Since the discovery of missense mutations in the chromosome 21 gene which encodes copper/zinc superoxide dismutase-1 (SOD1) in the dominantly inherited ALS family,[1–4] ALS research has focused on this SOD1 gene mutation.[5–9] A number of authors have proposed the possibility of programmed cell death, termed apoptosis, in the motor neurons in SOD1 transgenic mice, and suggested that the same cell death processes also occur in classic ALS in humans.

The definition of apoptosis is so fuzzy, however, as to confound attempts to interpret the results of apoptosis studies over a range of degenerative diseases. This lack of clarity is reflected in inconsistencies in the biochemical and morphological features of motoneuronal cell death observed in SOD1 transgenic mice and in patients with ALS.[10–16]

Several recent investigations of motor neuronal cell death in ALS have focused on caspases and related proteins in SOD1 transgenic mice.[17–20] Caspases are generated in the form of pro-enzymes (inactive form), and are activated by proteolysis to form active complexes which kill neurons via the apoptosis process. The caspases examined in the present study are thought to be associated with mitochondria and to be active in the final common pathway of the caspase cascade. Cytochrome C (Apaf-2) and Apaf-1 are discharged together from mitochondria, and form a complex with caspase-9 through caspase recruitment domain in the presence of dATP. As a result, caspase-9 is changed to the activated form, which in turn activates caspase-3, which finally induces cell death.

To clarify whether apoptosis is in fact associated with the cell death of motoneurons in ALS patients, we studied the presence of DNA fragmentation, the definitive sign of apoptosis, in these cells. In addition, we also analyzed Apaf-1 and caspase-9 mRNA, and immunocytochemically investigated Apaf-1 and caspase-3 in spinal motoneurons in ALS patients.

Correspondence: Mineo Yamazaki, MD, PhD, The 2nd Department of Internal Medicine, Nippon Medical School, 1-1-5 Sendagi, Bunkyo-ku, Tokyo 113-8602, Japan. Email: yamazaki@nms.ac.jp

Received 26 May 2005; accepted 30 May 2005.

MATERIALS AND METHODS

Tissue preparation

The brain and cervical and lumbar segments of the spinal cord were rapidly obtained at autopsy of patients with ALS ($n=3$), disease controls ($n=2$, ossification of the posterior longitudinal ligament and MSA) and non-neurological disease controls ($n=2$, acute myocardial infarction and adrenal gland cancer). All ALS patients showed symptoms of upper and lower motor neuron involvement and fulfilled the pathological criteria of ALS. The tissues obtained at autopsy were preserved, frozen at –80°C until analysis. For the TdT-mediated dUTP-biotin nick end-labeling (TUNEL) method, sections were made from formalin-fixed and paraffin-embedded blocks of the appropriate regions.

RT-PCR method

Total mRNA was isolated from the cerebral cortex (area 17), putamen and spinal cord of ALS patients. Poly A+ mRNA was controlled using a Quickprep mRNA purification kit (Amersham Pharmacia Biotech, Uppsala, Sweden). RT-PCR was performed using the following primers specific to *Apaf-1* and *caspase-9* genes. The sense and antisense primers for *Apaf-1* were 5′-ACATCACGAA TCTTTCCCGC-3′, corresponding to APPN, and 5′-AACACTTCACTATCACTTCC-3′, corresponding to APPC. The primers used for *caspase-9* were 5′-GCCATG GACGAAGCGGATCGGCGG-3′ (sense) and 5′-GGC CTGGATGAAAAAGAGCTGGG-3′ (antisense). PCR was performed with a synthetic first-strand cDNA template. Amplification was continued for 35 cycles (1 min denaturation at 94°C, 1 min annealing at 55°C, 2 min extension at 72°C).

Immunohistochemistry

Immunohistochemical staining was performed using mouse monoclonal anti-Apaf-1 antibody (MAB868; R & D systems, Minneapolis, MN, USA), rabbit polyclonal anti-CPP32 antibody[21] and mouse monoclonal anticaspase-3 antibody (sc-7272; Santa Cruz Biotechnology, CA, USA). Frozen sections were incubated with 3% hydrogen peroxide for 30 min to block endogenous peroxidase activity. The sections were incubated with the antibodies at 4°C overnight and immunoreactivity was visualized with a Histostain SP kit (Zymed, San Francisco, CA, USA).

TUNEL method

Formalin-fixed, paraffin-embedded lumbar cord specimens from six ALS patients were examined in comparison with those from four controls. To facilitate the earliest possible detection of changes in motor neurons, these six cases were selected from among more than 50 ALS cases for their relatively well-preserved anterior horn cells. Mean age of the ALS and control (three with cerebral infarction and one with Marchiafava-Bignami disease) patients was 67 years (range 50–84 years) and 50 years (range 18–70 years), respectively.

DNA fragmentation was detected by the TUNEL method, using an *in situ* cell death detection kit (Boehringer-Mannheim, Indianapolis, MN, USA). Negative controls were examined using TUNEL reaction solution without TdT or fluorescein dUTP. Feasibility of the nuclear labeling of cells by the TUNEL method was confirmed in intestinal tissue obtained at autopsy of patients with malignant lymphoma. After oligonucleosomal DNA cleavages were labeled, photos of each TUNEL-positive neuron were taken, the same specimens were stained with HE, and TUNEL-positive neurons identified from the

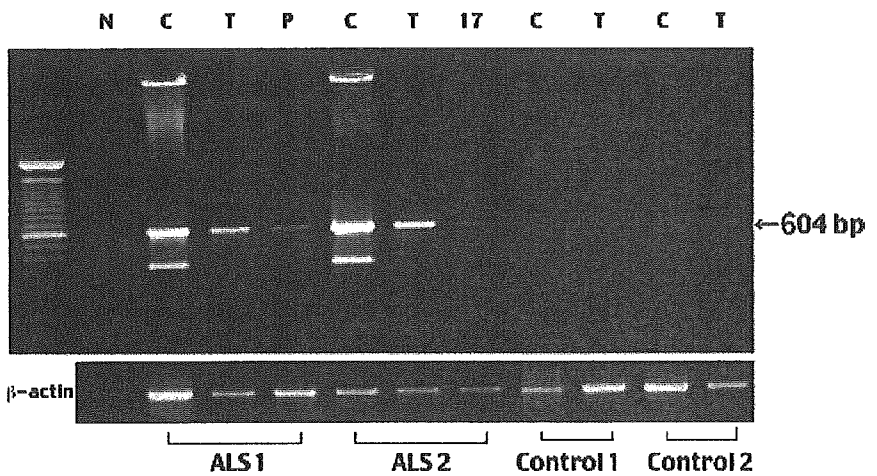

Fig. 1 Detection of Apaf-1 mRNA in the brains of control and ALS patients. β-actin mRNA in the same samples was used as control. The Apaf-1 mRNA band was detected in the cervical and thoracic cord, and was compared with cerebral cortex and putamen in patients with ALS (N: negative control, C: C8, T: Th12, P: putamen, 17: area 17).

photos were cytopathologically observed. TUNEL-positive spinal motor neurons and all anterior motor neurons in all sections were counted, and the frequency of TUNEL-positive spinal motor neurons was measured.

RESULTS

PT-PCR

PCR using primers to amplify *Apaf-1* clearly revealed positive bands of Apaf-1 mRNA in the cervical (C8) and thoracic cord (T12) in patients with ALS, but not in the cerebral cortex and putamen as such. In contrast, Apaf-1 mRNA was scarcely detected in the spinal cord of control cases (Fig. 1). Apaf-1 mRNA was clearly expressed in the putamen and cervical cord of patients with MSA (Fig. 2). The caspase-9 mRNA band was detected in the spinal cord of ALS patients and putamen and cervical cord of MSA patients, but was hardly seen in control cases (Fig. 3).

Immunocytochemistry

To determine whether Apaf-1 and caspase-3 are activated in ALS, control and ALS brains were immunostained with anti-Apaf-1 and anticaspase-3 antibodies. For Apaf-1, anterior horn motoneurons in control and ALS spinal cords showed weak cytoplasmic staining for Apaf-1, whereas ALS brains showed no significant differences to control brains (Fig. 4a,b). Immunolabeling using antibodies specific to caspase-3, rabbit polyclonal anti-CPP32 antibody (Fig. 4c,d) and mouse monoclonal anticaspase-3 antibody (Fig. 4e,f) revealed only scarce caspase-3 immunoreactivity in motor neurons in control and ALS brains.

TUNEL method

TUNEL-positive motor neurons in the anterior horn were observed in three of six ALS cases, whereas in control cases only two TUNEL-positive neurons were seen, one each in two cases. The TUNEL-positive motor neurons were atrophic and round in both groups, without large cell processes. They were filled with lipofuscin and the nucleus was eccentric, flat and pyknotic (Fig. 5a,b). Although TUNEL-positive motor neurons with Lewy body-like hyaline inclusions were occasionally found (Fig. 5c,d), no TUNEL-positive neurons carrying Bunina bodies were observed.

Not all atrophic anterior horn neurons were TUNEL-positive; some had TUNEL-negative nuclei, which were always a generally round shape with a light nucleoplasm. (Fig. 5e,f). However, most TUNEL-negative neurons were of normal size and had many processes in their cell bodies. TUNEL-positive motor neurons represented 5.3–8.9% of

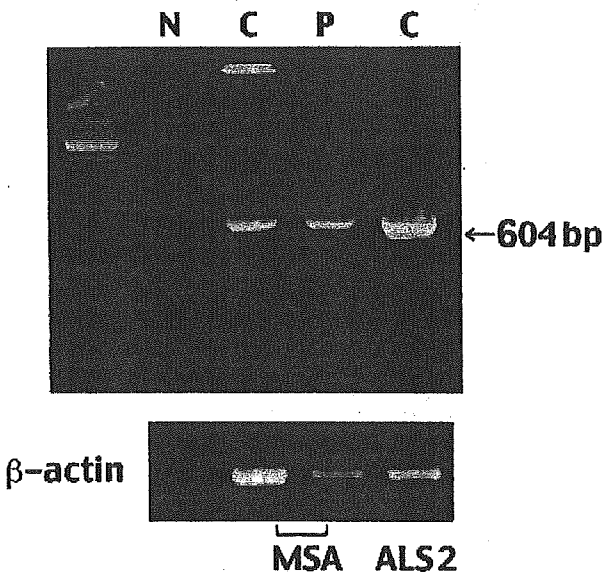

Fig. 2 Detection of Apaf-1 mRNA in the brains of MSA patients. Apaf-1 mRNA was expressed in the putamen and cervical cord of a patient with MSA (N: negative control, C: C8, P: putamen).

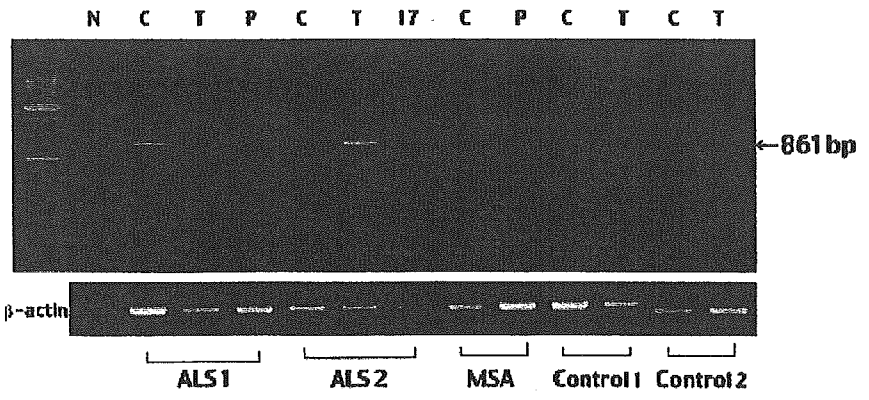

Fig. 3 Expression of caspase-9 mRNA in control, MSA and ALS brains. The caspase-9 mRNA band was detected in the spinal cord of ALS patients and in the putamen and cervical cord of MSA patients, but not in control case tissues (N: negative control, C: C8, T: Th12, P: putamen, 17: area 17).

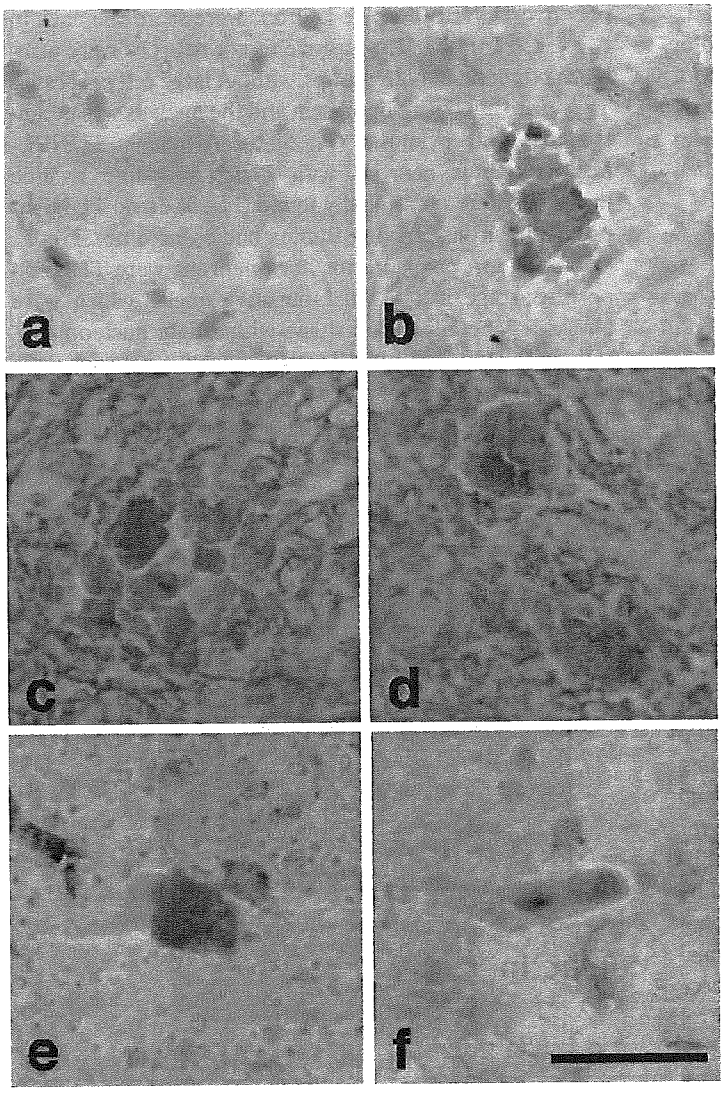

Fig. 4 Immunohistochemical expression of Apaf-1 and caspase-3 in the spinal cord of control and ALS patients. (a,b) No difference in Apaf-1 immunostaining between ALS (a) and control (b) cervical cords (C8). (c,d) Immunolabeling using rabbit polyclonal anti-CPP32 antibody showed no immunoreactivity in anterior horn neurons of control (c) or ALS (d) lumbar cords (L5). (e,f) Mouse monoclonal anticaspase-3 antibody revealed almost no immunoreactivity of caspase-3 in motor neurons in ossification of the posterior longitudinal ligament (e) or ALS (f) cervical cords (C8). Bar, 100 μm.

all anterior horn neurons (Table 1), and all motor neurons with a normal appearance were TUNEL-negative. No apoptotic bodies were seen in any ALS patient specimen.

DISCUSSION

For several reasons, the findings of this study on whether neurons in ALS undergo apoptosis were inconclusive. Although mRNAs of Apaf-1 and caspase-9 were apparently expressed in ALS brains, indicating that apoptosis through *Apaf-1* and *caspase-9* may be, at least to some extent, involved in this neuronal cell death, expression was not restricted to the ALS brain but was also recognized to some degree in the MSA brain. Further, we could not determine whether Apaf-1 mRNA and caspase-9 mRNA in the ALS brains were expressed by neurons, glia, or both. Indeed, our immunocytochemical investigation of Apaf-1, caspase-9 and caspase-3 failed to show any substantial increase in the production of these proteins in ALS over control brains. Against these findings, however, it was recently reported that caspase-9 is activated in spinal motor neurons of ALS patients.[22] It thus remains unclear whether caspase-9 is activated in motor neurons of ALS brains. In our study, caspase-9 mRNA was expressed in ALS brains and was clearly activated in motor neurons of the ALS spinal cord. However, our data also suggest that caspase-3 was not activated in the spinal motor neuron, and it was unlikely that the apoptotic cascade from caspase-9 to caspase-3 was present.

The phenomenon apoptosis was originally defined as fulfilling the following conditions: (i) DNA fragmentation;

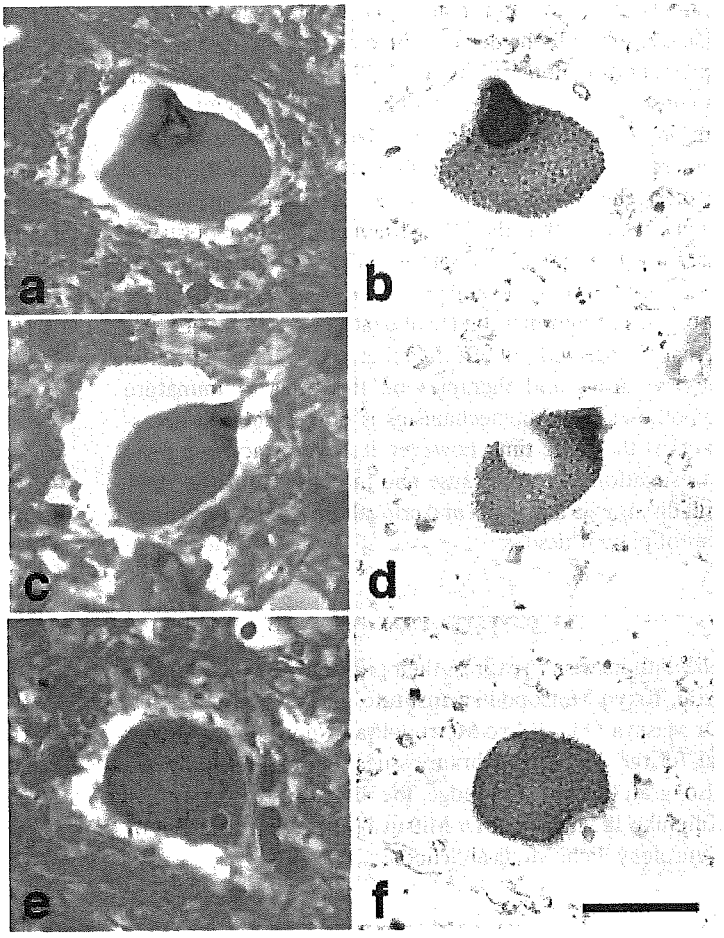

Fig. 5 TdT-mediateddUTP-biotinnickend-labeling (TUNEL) staining of anterior horn neurons in ALS patients. (a,b) A TUNEL-positive lumbar motor neuron is seen (case 1). The cell body is round and filled with lipofuscin. The same section stained with HE stain (a) and the TUNEL method (b). (c,d) TUNEL staining was occasionally observed in motor neurons with hyaline inclusions. (e,f) Some TUNEL-negative anterior horn neurons were atrophic and filled with lipofuscin. Bar, 50 μm.

Table 1 Positive TdT-mediated dUTP-biotin nick end-labeling (TUNEL) of ALS spinal motor neurons

Case	Age (years), sex	Total no. neurons (no.sections)	TUNEL-positive neurons	Mean % positive per section
1	61, female	486 (10)	26	5.3
2	81, female	219 (5)	13	5.9
3	67, male	202 (10)	18	8.9

and (ii) nuclear fragmentation and cellular budding (the presence of apoptotic bodies). Given the inconclusive PCR and immunocytology results here, we also checked whether the morphological changes of motor neurons in ALS were compatible with this definition. Results using the TUNEL method showed the presence of *in situ* DNA fragmentation in 5–9% of spinal motor neurons in ALS patients. If this DNA fragmentation does in fact represent a process of apoptosis, and if apoptotic cell death in motoneurons proceeds over a few hours as seen in other organs, this high proportion of TUNEL-positive cells would result in the total mathematical disappearance of spinal motor neurons in only a few months, with patients of course dying long before. In reality, however, the typical clinical course of several years before death means that one or both of the above assumptions is wrong. Although the possibility that apoptosis occurs more slowly in *in situ* motor neurons than other organ cells cannot be denied, *in vitro* studies using neuronal cell cultures[23] and our present finding that all TUNEL-positive neurons had shrunken pyknotic nuclei suggest that the mechanism of motor neuronal cell death in ALS represents a different process to apoptosis as defined above.

Moreover, it has been reported that the formation of apoptotic bodies was completed within several minutes in cells of a culture system.[24] Further, *in vivo*, apoptotic bodies disappear within only a few hours after formation in organs such as the liver.[25] If this is the case for motoneu-

rons also, this rapid time course may explain why apoptotic bodies can hardly be detected in human brain tissue. DNA fragmentation detected by the TUNEL method, however, is considered to represent an early stage of apoptosis, so specimens containing frequent TUNEL-positive neurons undergoing apoptosis should show at least some apoptotic bodies. This was not the case for our ALS specimens, implying again that the DNA fragmentation we observed may not be related to apoptosis. The present study thus fails to corroborate several reports indicating the apoptotic processes of motoneuronal cell death in ALS.[26–28] ALS is a lethal disease without effective therapy, so the exploration of new drugs and therapies on the basis of immature hypotheses of pathomechanisms is both valid and necessary. At the same time, however, it is necessary to pursue investigations into the cause and mechanism of this difficult disease via a rational and critical observation and analysis of patient tissues.

ACKNOWLEDGMENTS

The authors wish to express their gratitude to Dr Nobutaka Arai, Tokyo Metropolitan Institute for Neuroscience, and Dr Masaya Oda, Tokyo Metropolitan Neurological Hospital, for the donation of brain tissues used in this study. We also gratefully acknowledge the helpful support of Dr Kunihiko Ikeguchi and Dr Mitsuya Morita, Department of Neurology, Jichi Medical School.

REFERENCES

1. Deng HX, Hentati A, Tainer JA *et al.* Amyotrophic lateral sclerosis and structural defects in Cu, Zn superoxide dismutase. *Science* 1993; **261**: 1047–1051.
2. Aoki M, Ogasawara M, Matsubara Y *et al.* Mild ALS in Japan associated with novel SOD mutation. *Nat Genet* 1993; **5**: 323–324.
3. Elshafey A, Lanyon WG, Connor JM. Identification of a new missense point mutation in exon 4 of the Cu/Zn superoxide dismutase (SOD-1) gene in a family with amyotrophic lateral sclerosis. *Hum Mol Genet* 1994; **3**: 363–364.
4. Nakano R, Sato S, Inuzuka T *et al.* A novel mutation in Cu/Zn superoxide dismutase gene in Japanese familial amyotrophic lateral sclerosis. *Biochem Biophys Res Commun* 1994; **200**: 695–703.
5. Gurney ME, Pu H, Chiu AY *et al.* Motor neuron degeneration in mice that express a human Cu, Zn superoxide dismutase mutation. *Science* 1994; **264**: 1772–1775.
6. Tsuda T, Munthasser S, Fraser PE *et al.* Analysis of the functional effects of a mutation in SOD1 associated with familial amyotrophic lateral sclerosis. *Neuron* 1994; **13**: 727–736.
7. Dal Canto MC, Gurney ME. Development of central nervous system pathology in a murine transgenic model of human amyotrophic lateral sclerosis. *Am J Pathol* 1994; **145**: 1271–1279.
8. Durham HD, Roy J. Dong L, Figlewicz DA. Aggregation of mutant Cu/Zn superoxide dismutase proteins in a culture model of ALS. *J Neuropathol Exp Neurol* 1997; **56**: 523–530.
9. Ghadge GD, Lee JP, Bindokas VP *et al.* Mutant superoxide dismutase-1-linked familial amyotrophic lateral sclerosis: molecular mechanisms of neuronal death and protection. *J Neurosci* 1997; **17**: 8756–8766.
10. Migheli A, Cavalla P, Marino S, Schiffer D. A study of apoptosis in normal and pathologic nervous tissue after in situ end-labeling of DNA strand breaks. *J Neuropathol Exp Neurol* 1994; **53**: 606–616.
11. Rabizadeh S, Gralla EB, Borchelt DR *et al.* Mutations associated with amyotrophic lateral sclerosis convert superoxide dismutase from an antiapoptotic gene to a proapoptotic gene: studies in yeast and neural cells. *Proc Natl Acad Sci USA* 1995; **92**: 3024–3028.
12. Troost D, Aten J, Morsink F, de Jong JMBV. Apoptosis in amyotrophic lateral sclerosis is not restricted to motor neurons. Bcl-2 expression is increased in unaffected post-central gyrus. *Neuropathol Appl Neurobiol* 1995; **21**: 498–504.
13. Troy CM, Shelanski ML. Down-regulation of coper/zinc superoxide dismutase causes apoptotic death in PC12 neuronal cells. *Proc Natl Acad Sci USA* 1994; **91**: 6384–6387.
14. Yoshiyama Y, Yamada T, Asanuma K, Asahi T. Apoptotic related antigen, LeY and nick-end labeling are positive in spinal motor neurons in amyotrophic lateral sclerosis. *Acta Neuropathol* 1994; **88**: 207–211.
15. Mu X, He J, Anderson DW, Trojanowski JQ, Springer JE. Altered expression of bcl-2 and bax mRNA in amyotrophic lateral sclerosis spinal cord motor neurons. *Ann Neurol* 1996; **40**: 379–386.
16. Martin LJ. Neuronal death in amyotrophic lateral sclerosis is apoptosis: possible contribution of a programmed cell death mechanism. *J Neuropathol Exp Neurol* 1999; **58**: 459–471.
17. Pasinelli P, Borchelt DR, Houseweart MK, Cleveland DW, Brown RH Jr. Caspase-1 is activated in neural cells and tissue with amyotrophic lateral sclerosis-associated mutations in copper-zinc superoxide dismutase. *Proc Natl Acad Sci USA* 1998; **95**: 15763–15768.
18. Li M, Ona VO, Guegan C *et al.* Functional role of caspase-1 and caspase-3 in an ALS transgenic mouse model. *Science* 2000; **288**: 335–339.